Modeling Reveals the Role of Coastal Upwelling and Hydrologic Inputs on Biologically Distinct Water Exchanges in a Great Lakes Estuary

Qianqian Liu[1,2], Eric J. Anderson[3*], Yinglong Zhang[4], Anthony D. Weinke[1], Katie L. Knapp[1], Bopaiah A. Biddanda[1]

[1] Annis Water Resources Institute, Grand Valley State University, Muskegon, MI 49441, USA

[2] Cooperative Institute for Great Lakes Research, University of Michigan, Ann Arbor, MI 48018, USA

[3] Great Lakes Environmental Research Laboratory, National Oceanic and Atmospheric Administration, Ann Arbor, MI 48018, USA

[4] Virginia Institute of Marine Science, Gloucester Point, VA 23062, USA

Manuscript submitted to: *Estuarine, Coastal and Shelf Science*

Abstract

Freshwater estuaries everywhere are under stress from anthropogenic activities and climate change. Muskegon Lake Estuary (MLE) is a freshwater estuary along the eastern shore of Lake Michigan characterized by algal blooms and hypoxia during the summer and designated as an Area of Concern (AOC) by the EPA. We developed a 3-D hydrodynamic model using the Semi-implicit Cross-scale Hydroscience Integrated System Model (SCHISM) to study the hydrodynamics of MLE with a focus on the cold-water intrusions from Lake Michigan into MLE. Substantial water exchange process was validated by comparisons with observations in the near-shore region of Lake Michigan and in the navigation channel between Lake Michigan and MLE. The model found that the cold-water intrusions from Lake Michigan to MLE occur during summer stratification, amounting to as much as 10% of MLE's total volume during one single episodic event. The intrusion was accompanied by a stronger surface outflow in the opposite direction, which may accelerate the delivery of MLE water to Lake Michigan. Through process-oriented model experiments, we examined the cold-water intrusion's responses to hydrological shift under climate change, and found that the increase in riverine input during upwelling weakens the intrusion. In addition, an increase of navigation channel width strengthens the cold-water intrusion, and that intrusion strength as well as intrusion period was directly related to wind speed. Our observation-modeling based findings would provide a good reference for the future study of biophysical interactions between coastal ocean and estuaries.

Keywords: freshwater estuary; cold-water intrusion; upwelling; hydrologic shift; numerical model; hypoxia

1. Introduction

Estuaries are an ecologically active interface between riverine systems and coastal waters, which provide unique habitats for many varieties of plants and animals, are highly productive systems, and undergo several complex biological and physical processes. Similar to brackish estuarine systems, freshwater estuaries involve mixing of chemically and biologically distinct waters, as they receive hydrologic inputs with carbon and nutrients from terrestrial sources and heavily urbanized population centers, and as a result can have large spatial variability in dissolved oxygen, conductivity, and turbidity (Fisher et al., 2015). Such land-water interface ecosystems are greatly affected by anthropogenic activities and climate change (Borja et al., 2010).

Though extremely large, the Laurentian Great Lakes, are quite vulnerable to anthropogenic stressors and climate driven changes in physical or biogeochemical conditions such as thermal stratification, precipitation and runoff, and timing of the hydrometeorological cycle (Allan et al. 2012; Larson et al., 2013; Cotner et al. 2017). In addition, lakes are highly reactive sites for carbon metabolism and play a critically important role in the global carbon cycle because of the enhanced rates of carbon respiration and burial within them (Cole et al., 2007; Tranvik et al., 2009; Biddanda 2017). As climate projections reveal intensification of extreme precipitation events over the next century (Donat et al., 2016; Wang et al., 2017), and subsequent shifts in riverine inputs to estuarine systems, an important concern arises regarding the impact of these changes on estuarine function – such as rising coastal eutrophication worldwide (Sinha et al. 2017).

Extensive studies have focused on the mechanisms that control estuarine dynamics, including the exchange flow in different brackish estuarine systems (Chen et al., 2012), the generation of estuarine front (Geyer and Ralston, 2015; Liu et al., 2016a, b), turbulent mixing in

61 estuaries and the resulting variations in water exchange (Simpson et al., 1990; Rong and Li, 2012;
62 Liu et al., 2017), and biologically distinct water exchange during coastal upwelling (Roegner, et
63 al., 2011). Roegner et al. (2011) found that the coastal upwelling supplies oxygen-depleted water
64 to the Columbia River estuary and therefore deteriorates the estuarine habitats. Similarly,
65 upwelling along the central California coast supports Harmful Algal Blooms (HABs) in some
66 open embayments by delivering nutrients from the bottom of the coastal ocean to the
67 embayments but sustaining its stratification (Pitcher et al., 2010). Along the California coast, in
68 2007, an inshore anoxia over a 5 km stretch of coastline at Erendira is believed to be caused by a
69 strong upwelling region off Baja California, killed many animals, including tons of lobsters
70 (Levin et al., 2009). Intrusions of saline hypoxic water to estuaries are commonly found, for
71 example, from the ocean to Puget Bay (Deppe, 2017), from Gulf of Mexico to its embayments
72 (Rabalais, 2002), and from Chesapeake Bay to the lower reaches of the Choptank River
73 (Breitburg, 1992; Breitburg, 2002; Sanford et al., 1990). Similar intrusions of cold, dense
74 oxygenated waters have also been found to occur in the freshwater estuaries of the Great Lakes;
75 e.g., Lake Michigan water into Green Bay (Grunert, 2013) and Lake Ontario water into Hamilton
76 Harbor (Lawrence et al., 2004), and the Muskegon Lake Estuary (MLE; Biddanda et al., 2018),
77 the investigation area in this study.

78 In the Great Lakes, where tides are weak, winds become the dominant mechanism for
79 water exchange between the Great Lakes and freshwater estuaries. However, there is little
80 information on the drivers of exchange in a freshwater estuary and in particular, how the
81 mechanisms that control important ecological variables such as dissolved oxygen are impacted
82 by shifts in precipitation or meteorology due to a changing climate. To investigate the dominant
83 mechanisms behind freshwater estuary exchange and the sensitivity of spatiotemporal variability

84 of dissolved oxygen to these controls, this study focuses on the MLE, one of the several drowned
85 river-mouth estuaries along the eastern coastline of Lake Michigan (Larson et al. 2013).
86
87 **2. Study Area**
88 The MLE is a mesotrophic drowned river mouth along the eastern shore of Lake
89 Michigan (Fig. S1 in Supplementary Material), with a surface area of 17 km^2, a water volume of
90 119 million m^3, a mean water depth of 7 m, a maximum depth of 21 m (Fig. 1; Steinman et al.,
91 2008; Marko et al., 2013) and an average hydraulic residence time of 23 days. The estuary drains
92 the second largest watershed in Michigan (approximately 7,302 km^2) including 53.2% forested,
93 23.0% agricultural, and 4.2% urban lands (Marko et al., 2013), and connects to an oligotrophic
94 Lake Michigan through a 1 km long and 100 m wide navigation channel.
95 Historical observations show that the MLE is under the effects of anthropogenic activities
96 and climate change (Steinman et al., 2008). The proportion of urbanized land within the
97 Muskegon River watershed is projected to increase by 11.5% by the year 2040 (Tang et al.,
98 2005), which changes the nature and quantity of nutrients, major ions, and dissolved organic
99 carbon (DOC) inputs to the estuary. The US Geological Survey (USGS;
100 http://waterdata.usgs.gov/nwis) has recorded stream flows within the watershed since the early
101 20^{th} century. Over most of that period, gauged flow of the Muskegon River from USGS, which is
102 the primary input to the estuary, shows an increase of 34% in mean flow, 16% in low flow, and
103 10% in peak flow since monitoring began in 1935. Wiley et al. (2010) showed an increase in the
104 base flow, storm flow, and median discharge by 15-20% in BAU (end of century with business
105 as usual land management) scenario under the current climate regime.

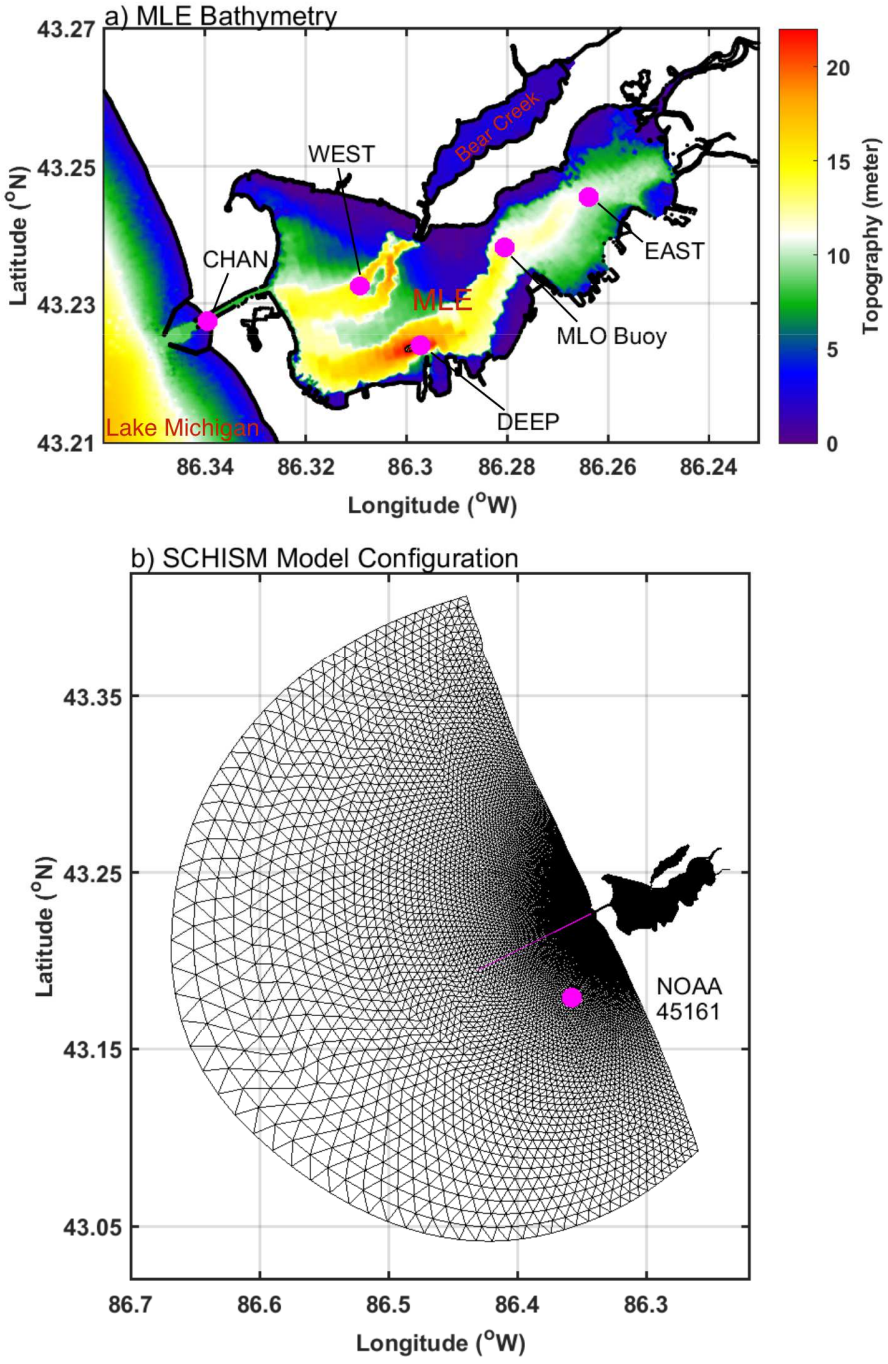

106

107 Figure 1. a) Bathymetry of Muskegon Lake Ecosystem (MLE) with observing buoy locations,
108 and (b) coastal Lake Michigan with Semi-implicit Cross-scale Hydroscience Integrated System
109 Model (SCHISM) configuration.

110

111 The MLE was listed as an EPA AOC in 1985 due to historical contamination and habitat
112 degradation. Recent observations in the MLE and previous annual samplings have revealed an
113 annually recurring lake-wide hypoxia (Biddanda, 2012; Biddanda et al., 2018), and the potential
114 for hypolimnetic habitat degradation and increased eutrophication due to sediment phosphorus
115 release (Steinman et al., 2008; Weinke and Biddanda, 2018).

116 Preliminary results from observations suggest that hypoxia in the estuary is mitigated by
117 episodic cold-water intrusion from Lake Michigan during coastal upwelling events under certain
118 wind conditions (Biddanda, 2018). Water temperature and dissolved oxygen throughout the
119 water column were measured by the Muskegon Lake Observatory (MLO; Fig. 1a) each year
120 from April/May to November/December since 2011 (Biddanda 2012; Biddanda et al., 2018;
121 www.gvsu.edu/buoy). Physically, MLO observations revealed that the cold-water intrusion
122 strengthens MLE's stratification in the middle of July, August, and early September as shown in
123 Fig. S3a. Ecologically, the dissolved oxygen saturation (Fig. S3b) showed that the hypoxia is
124 mitigated by the cold-water intrusion with increased dissolved oxygen concentrations during the
125 intrusion.

126 The cold-water intrusion's influence on the ecosystem is more complex than what is
127 revealed from a single station due to the spatial variations in nutrients and seston from the
128 Muskegon River to Lake Michigan. Observations at five fixed stations in MLE and the near
129 shore zone of Lake Michigan from March to October 2003 exhibited explicit spatial variations in
130 nutrient concentrations and seston stoichiometry from the Muskegon River to Lake Michigan
131 (Marko et al., 2013). Much of the terrestrial material from the Muskegon River was intercepted
132 and processed by MLE before flowing into Lake Michigan. Therefore, generally, levels of
133 organic matter (including dissolved organic carbon and particulate organic carbon), total

suspended matter, and total phosphorus contained in the fine-grain sediment is consistently lower in Lake Michigan than those observed in MLE (Marko et al., 2013). Stratification combined with the high amount of organic matter in MLE leads to episodic hypoxia in the estuary (Biddanda et al., 2018), while such an event is infrequent in Lake Michigan. As another major spatial difference, because Lake Michigan has phosphorus limitation to phytoplankton growth (Hecky et al., 1993), the mean C:P ratio was much higher in Lake Michigan than MLE due to the lower phosphorus concentrations in Lake Michigan. Thus, water exchange between the Great Lakes and freshwater estuaries is closely associated with nutrients/organic matter redistribution.

In light of the significance of cold-water intrusions to water exchange between the Great Lakes and freshwater estuaries, modeling of cold-water intrusions and its response to different factors is valuable for the understanding of estuarine ecosystems. In this work, we investigate the processes that govern exchange in a freshwater estuary. Through the combination of a long record of observations in the MLE and the development of a hydrodynamic model, we explore the dynamics behind dense water intrusion to freshwater estuaries during coastal upwelling, as well as the intrusion's response to shifts in hydrologic inputs that would result under changing precipitation patterns as a result of climate change. Finally, we test the sensitivity of the dense water intrusion to anthropogenic activities such as alterations to the navigation channel that connects the estuary to the coastal waters.

3. Methods

3.1 Model Description

To understand the physical processes that govern exchange in the MLE, a three-dimensional hydrodynamic model has been developed for MLE, which extends from the mouth of the Muskegon River to the offshore of Lake Michigan (Fig. 1). The model is based on the Semi-implicit Cross-scale Hydroscience Integrated System Model (SCHISM; Zhang et al., 2011, 2015, 2016), an open-source community-supported modeling system based on unstructured grids, derived from the early SELFE model (Zhang and Baptista 2008). It employs a highly efficient and accurate semi-implicit finite-element/finite-volume method with Eulerian-Lagrangian algorithm to solve the Navier-Stokes equations, and has been widely applied to bays and estuaries around the world (Zhang et al., 2015; Liu et al., 2017; Chao et al., 2017). The model uses the two-equation closure schemes from the GLS model of Umlauf and Burchard (2003) with the stability function by Kantha and Clayson (1994), and a quadratic bottom drag formulation for bottom stress. The model domain includes Muskegon Lake and the eastern coast of Lake Michigan at the mouth of MLE (Fig. 1b) with horizontal resolution ranging from approximately 2 km in the coastal area in Lake Michigan to as high as 25 m in the navigation channel and MLE, and vertical resolution defined by 20 terrain-following sigma layers. Model bathymetry and coastline topography were provided by NOAA global relief (ngdc.noaa.gov) and Electronic Navigation Charts (encdirect.noaa.gov).

Unlike in most coastal ocean systems, tides in the Great Lakes are weak, and thus the dominant mechanism for transport is the surface wind field, which produces episodic circulation patterns, storm surges, and seiches (Mortimer, 2004). In Lake Michigan, long-term observations found cyclonic circulations in summer and increased cyclonic circulation in winter, important for the transport pathways of nutrients and contaminants on long time scales (Beletsky et al., 1999). In order to account for the complex hydrodynamics in Lake Michigan and the impact on the

178 estuary, the MLE model uses a one-way nesting approach from the NOAA Lake Michigan-
179 Huron Operational Forecast System (LMHOFS; Anderson and Schwab, 2017;
180 https://tidesandcurrents.noaa.gov/ofs/glofs.html).

181 Hourly surface forcing is prescribed from the Great Lakes Coastal Forecasting System
182 (GLCFS; Schwab and Bedford, 1994), which provides spatially varying wind, air temperature,
183 humidity, long wave and short wave radiation. The GLCFS uses real-time coastal observations
184 from around the Great Lakes to generate a spatially-interpolated meteorological field that is
185 accurate for over-lake conditions. The major hydrologic input to the MLE is from the Muskegon
186 River, which drains the second largest watershed in Michigan and connects at the eastern side of
187 the lake. Hourly river discharge from the USGS Croton Dam station, which is located 52 km
188 upstream from the river mouth, is scaled using an area-ratio method of the total and the gauged-
189 portion of the watershed.

190 **3.2 Numerical Experiments Design**

191 A control case simulation was carried out for the period January 1 – December 31, 2016
192 using lateral and surface boundary conditions as described above, and initialized with a constant
193 water temperature at 2 ^{o}C. This period covers the formation of thermal stratification in the early
194 summer, several upwelling-induced cold-water intrusion events during the stratified period, and
195 thermal mixing and overturning in the fall. Modeled thermal structure and currents were
196 compared to observations within the MLE at CHAN, WEST, DEEP and DEEP sites (Fig. 1a)
197 and along the shore of Lake Michigan at NOAA station 45161 (Fig. 1b). Observations at the
198 MLE sites were sampled every hour for water quality parameters and temperature; at NOAA
199 station 45161, temperature and currents are sampled every 20 minutes. In addition, a series of
200 idealized experiments were carried out to examine the response of cold-water intrusion to

different factors (Table 1). The idealized experiments were focused on a period of significant cold-water intrusion that occurred in September. In each case, the model was restarted from August 28 using initial conditions from the control case simulation.

To examine the response of cold-water intrusion to shifts in hydrologic inputs under changing precipitation patterns (Wang et al., 2017), in experiments R1, R2, R3 and R4, the variations in river discharge were simulated by multiplying the flow from August 28 to December 31 by 0.5, 2, 3 and 4 times with averaged flow rates during the intrusion of 20, 80, 120 and 160 m^3/s, respectively. Fig. S2 shows the historical discharge observations from 1996 to 2016, demonstrating the inter-annual variability of hydrologic input in summer when the water in Lake Michigan and the MLE is stratified. While climate projections suggest intensification and shift of extreme precipitation events over the next century (Donat et al., 2016; Wang et al., 2017), the cases R3 and R4 are used to examine the change of cold-water intrusion under climate projection including intensification and shift of extreme precipitation events.

Anthropogenic activities may affect the coastal ocean, estuaries and lakes with many stressors including urbanization and runoff, agriculture, microbial processing of organic matter and nitrification/denitrification (Hoffman et al., 2014), as well as shoreline modifications such as shoreline engineering, dune destruction, channel dredging and jetty construction. Even though the navigation channel is unlikely to change in MLE, the influence of navigational channel characteristics on hydrodynamic and ecological processes is relevant to extending this work to other similar systems. In addition, previous studies have suggested that the potential for Lake Michigan waters to flow into MLE is limited due to the narrow connection in the channel (Marko et al., 2013), and thus our work aims to verify those conclusions. In experiments N1, N2 and N3, the impact of the navigation channel was evaluated by broadening its width by 2, 3, and 4 times,

224 respectively.

225 Finally, the strength of upwelling and consequent extent of cold-water intrusion depends
226 on the wind stress and nearshore bathymetry. To investigate the intrusion's response to
227 upwelling strength under prevailing alongshore winds with different magnitudes (Table 1),
228 experiments W1-4 are undertaken. In each case, prevailing alongshore upwelling-favorable
229 winds are applied for the period August 28-30 at 3 m/s, 5 m/s, 7 m/s and 15 m/s, respectively,
230 followed by no wind for 10 days.

Run	Width of Navigation Channel	River Discharge	Wind Speed
Ctrl case	Real	Real	Real
R1	Real	Half	Real
R2	Real	2 times	Real
R3	Real	3 times	Real
R4	Real	4 times	Real
N1	2 times	Real	Real
N2	3 times	Real	Real
W1	Real	Real	Alongshore winds; 3 m/s [a]
W2	Real	Real	Alongshore winds; 5 m/s
W3	Real	Real	Alongshore winds; 7 m/s
W4	Real	Real	Alongshore winds; 15 m/s

231 a. The alongshore winds in W1, W2, W3 and W4 are upwelling favorable, i.e., northwesterly, for the first
232 three days, after three days, there is no wind applied.

233 Table 1. Process-oriented experiments for the study of intrusion length.

234 **4. Results and Discussion**

235 **4.1 Model Assessment**

236 Before analyzing model results from the idealized experiments, the control case
237 simulation was first validated by comparing with available observations to establish confidence
238 in the model. To verify the modeled stratification and currents in Lake Michigan, comparisons
239 were made with measured temperature and velocities at NOAA station 45161 (Figs. 2a, 2b).
240 Currents are observed at NOAA 45161 from 2.5 meter to 20.5 meter depth with a bin of 1 meter.
241 We compared the daily-averaged, model currents with the observations (Fig. 2a) at selected

depths throughout the water column.

According to Fig. 2a, the modeled currents are consistent with observations in amplitude and change of direction with root mean square errors (RMSEs) of 5.30, 4.44, 3.77, 3.03 and 2.53 cm/s for u-component velocity at 2.5, 7.5, 12.5, 17.5 and 20.5 m below the surface, and 10.5, 9.39, 7.09, 4.40 and 3.12 cm/s for v-component (Table 2). When upwelling-favorable winds occur during the beginning of August and September, the model captures the strong surface currents moving southeastward. The currents decrease with depth and reverse at a depth. For example, the current reverses at the depth of 12.5 m at the beginning of August. To further evaluate model performance and the hydrodynamics in the nearshore, additional statistical measures are included to be consistent with previous studies of Lake Michigan (Eqs. 1-4; Schwab, 1983; Beletsky and Schwab, 2001; Anderson and Schwab, 2011; Table 2).

$$\sigma_{ou}=\frac{\sum[(u_{ou}\,u_o\quad(v_{ou}\,v_{ou}\ ]u}{\sum(u_{ou}\quad v_{ou}} \tag{1}$$

$$\sigma_{cu}=\frac{\sum[(u_{cu}\,u_c\quad(v_{cu}\,v_{cu}\ ]u}{\sum(u_{cu}\quad v_{cu}} \tag{2}$$

$$\varepsilon=\frac{\sum[(u_o\quad u_{ou}\,u_{cu}\,u_{cu}\quad(v_{ou}\,v_{ou}\,v_{cu}\,v_{cu}\ ]u}{\sum[(u_{ou}\,u_{ou}\quad(v_{ou}\,v_{ou}\ ]u} \tag{3}$$

$$\|v_o,v_c\|=\left(\frac{1}{n}\sum_{t=1}^{n}|v_{ou}-v_c|^2\right)^{1/2} \qquad F_{nu}=\frac{\|v_o,v_c\|}{\|v_o,0\|} \tag{4}$$

where ($_o$, v_o) represent observed current, and ($_c$, v_c) represent modeled (computed) current.

$\sigma_{ou}(\sigma_c)$ is the ratio of energy in the time-variable component of the currents to the total current energy for observed (modeled) currents. With values from 0.84 to 1.00 at NOAA 45161 (Table 2), it describes the nearshore of Lake Michigan as wind-dominated with a higher ratio of energy in the time-variable component of the currents to the total current energy.

The differences between observed and modeled currents for the time-variable flow are measured by ε. A value of 0.0 indicates a perfect match between the observed and modeled

currents, and a value of 1.0 indicates an error in the modeled current as large as the observed current. According to previous studies (Schwab, 1983; Schwab and Bennett, 1987; Anderson and Schwab, 2011), a value 0.9 is typical for the time-variable component in the Great Lakes, as the observed currents can contain substantial energy beyond the model resolution. Therefore, prediction with $\varepsilon \leq 0.9$ is considered successful.

F_n, a normalized Fourier norm, describes the relative percentage of variance in the observed currents that is unexplained by the modeled currents. If $F_{nu} = 0$, the model has perfect prediction; If $0 < F_{nu} < 1$, the model prediction is better than no prediction at all. For a reference, Schwab (1983) got $0.79 < F_{nu} < 1.01$ for a barotropic simulation of Lake Michigan currents on a 5-km grid. Beletsky and Schwab (2001) calculated $0.5 < F_{nu} < 0.9$ for the Lake Michigan coastal current prediction in winter also on a 5-km grid.

At NOAA 45161, with ε_u around 0.5 throughout the water column, and both F_{uu} (F_{nu} for the u-component velocity) and F_{vu} (F_{nu} for the v-component velocity) around 0.7, the model is found to predict nearshore currents in Lake Michigan on par with previous studies.

Depth (m)	RMSE_u (cm/s)	RMSE_v (cm/s)	σ_{ou}	σ_{cu}	ε	F_{uu}	F_{vu}
2.5	5.30	10.50	0.94	0.97	0.49	0.69	0.70
7.5	4.44	9.39	0.96	1.00	0.51	0.70	0.75
12.5	3.77	7.09	1.00	0.97	0.50	0.70	0.73
17.5	3.03	4.40	0.94	0.95	0.49	0.68	0.68
20.5	2.53	3.12	0.84	0.97	0.49	0.66	0.74

Table 2. Comparisons of modeled and observed currents at NOAA 45161.

Fig. 2b shows the comparison of surface and bottom temperature at NOAA 45161 during

May 2016 to November 2016 with RMSEs of 1.4°C and 3.1°C respectively. The surface temperature captures the seasonal trend shown in the observations, and the major events, such as the episodic, abrupt decrease in temperature around June 6, July 2, August 3, and September 2. The model slightly overestimates the bottom temperature, which may arise from a diffuse resolution of the thermocline from the LMHOFS model or from the lack of groundwater flux in the model, which is more obvious in the comparisons of bottom temperature inside MLE.

With respect to conditions inside the MLE, Fig. 2c shows the comparisons of surface and bottom temperature at the station CHAN with RMSEs of 0.6°C and 2.8°C, respectively. In particular, the bottom temperature in the channel reveals the model's ability to capture the intrusion events driven by upwelling in Lake Michigan. However, further inside the MLE, it is a more complicated situation. The model's surface temperature closely follows the observations at the DEEP station, with RMSE of 0.7°C, however, the bottom temperature is highly overestimated (Fig. 2d) with a RMSE of 5.8°C (similar to other stations in MLE; Fig. S4 in the Supplementary Material). A possible explanation for the discrepancy in bottom water temperature within the MLE could be the inclusion of groundwater inflow to the system. In a similar nearby system, Gull Lake, Safaie et al. (2017) showed groundwater input to be a critical feature to capturing the thermal stratification. Thus, in a simulation of the control case with groundwater inflow included, based on rough approximations of flux and temperature, the model reveals a better resolution of bottom water temperatures within the MLE (Figs. S7-S9 in the Supplementary Material), suggesting that this might be a reasonable culprit and worthy of further investigation. However, in the absence of accurate groundwater information, and since the difference in model results with and without groundwater included are small or negligible in terms of the model's ability to resolve water exchange and the cold-water intrusions driven by

upwelling in Lake Michigan, the following model simulations are shown for the control case without groundwater. Further discussion can be found in section 4.7 and in the Supplementary Material.

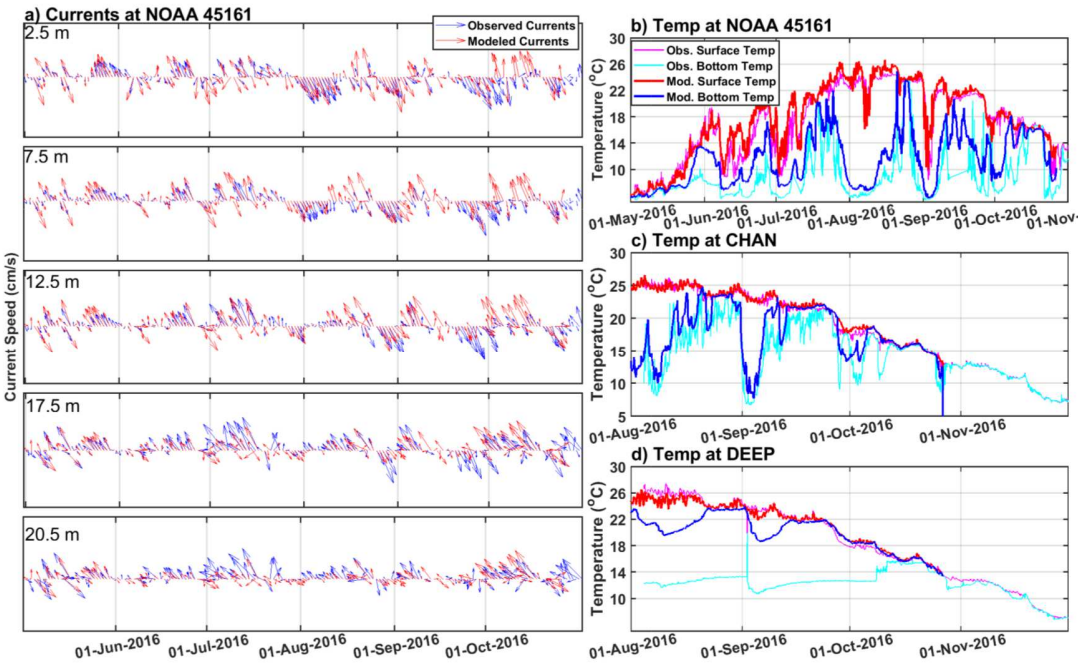

Figure 2. Comparisons of currents and temperature between model and observations including a) currents at station NOAA 45161 in Lake Michigan at 2.5, 7.5, 12.5, 17.5 and 20.5 meters below surface, surface and bottom temperature b) at NOAA 45161, c) at station CHAN inside the navigation channel, and d) at station DEEP. The arrow direction in a) represents the current direction with an arrow pointing northward for a northward current.

4.2 Cold-water intrusion

Along the eastern boundary of Lake Michigan, southward alongshore winds induce Ekman transport (Ekman, 1905) of surface water away from the shore. These displaced surface waters are replaced by deeper Lake Michigan waters, resulting in coastal upwelling often characterized by cold surface waters at the coast (Plattner et al., 2006). Surface temperature from the LMHOFS model in 2016 (Fig. 3a) reveals periodic occurrence of upwelling along the eastern

shore of Lake Michigan with surface temperature decreasing to below 18°C on September 2 and 4, when the lake is stratified, and upwelling-favorable winds develop (Fig. 3b). Again, on September 11, northerly winds occur, though with a much shorter duration than the event beginning on September 1 (Fig. 3b). Correspondingly, there is a weaker upwelling with surface temperature around 20.5°C (Fig. 3a). Historical observations inside the navigation channel between Lake Michigan and MLE show colder bottom temperatures during these upwellings events (Fig. 3c).

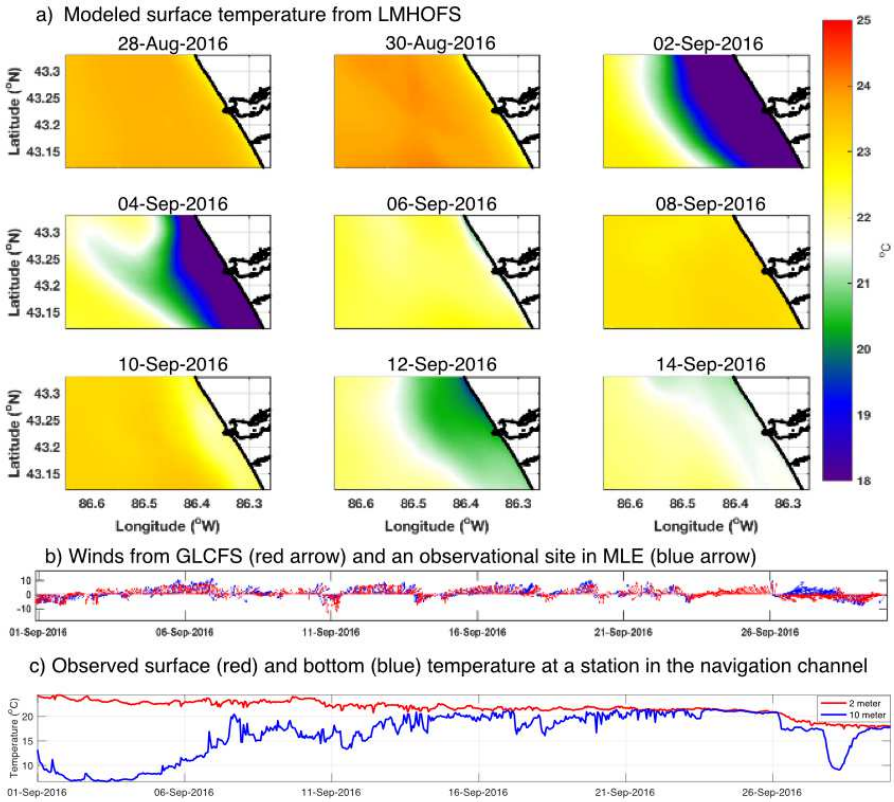

Figure 3. a) Daily averaged surface temperature from August 28, 2016 to September 14, 2016 during an upwelling event from the LMHOFS model; b) Winds in MLE in September 2016 with red arrow represents the data used by GLCFS and blue arrow represents the observations at the GVSU buoy site (http://www.gvsu.edu/wri/buoy/); c) observed near surface and bottom temperature in September 2016 at a station inside the navigation channel.

Taking the large upwelling in September as a representative event to investigate the cold-water intrusion in MLE and its effects to the hydrodynamics of MLE, we plotted the daily averaged bottom temperature in MLE from August 31, 2016 to September 10, 2016 (Figs. 4a-f). Model simulations of temperature and along-channel velocity at CHAN (Figs. 4 g-i) demonstrate that the episodic occurrence of bottom cold-water in Figs.2 and 3 is due to the cold-water intrusion from Lake Michigan to Muskegon Lake during upwelling-favorable winds (Fig. 3b).

On August 28 and 29, before the upwelling, the water column at the NOAA station 45161 was highly stratified with surface temperature higher than 20^{o}C (Fig. 4g). The subsurface water temperature fluctuates with a period of ~17 (about 17.2) h, which is caused by the oscillations of rotation-modified internal (Poincaré) wave (Schwab, 1977; Beletsky et al., 1997). Poincaré waves are a travelling disturbance of the wind-induced upwelling/downwelling perturbations of the thermocline on a whole-basin scale (Schwab, 1977; Mortimer, 1984). They are characterized by clockwise phase progression with a period slightly less than the local inertial period, $2\pi/f$ (f is Coriolis parameter), 17.5 h for Central Michigan. Spectral analysis of water elevation reveals the oscillation also occurs in the navigation channel and inside MLE, although its influences to the temperature profile in the channel are negligible (Figs. 4h) - the navigation channel is well mixed with temperature higher than 20^{o}C through the water column. Before the upwelling, along-channel velocity inside the navigation channel is characterized by a high frequency oscillation with a period of 3.25 hr (or 3.4, 3.6 hr for different time), which is corresponding to the third longitudinal seiche mode in Lake Michigan (Mortimer, 2004). Spectral analysis of our model results shows the oscillation occur in both Lake Michigan and MLE, but relatively stronger in MLE. However, the seiche is not strong enough to affect the

reversals in water exchange within the channel. Currents in the channel move from MLE to Lake Michigan through the water column with a speed about 10 cm/s (Fig. 4i).

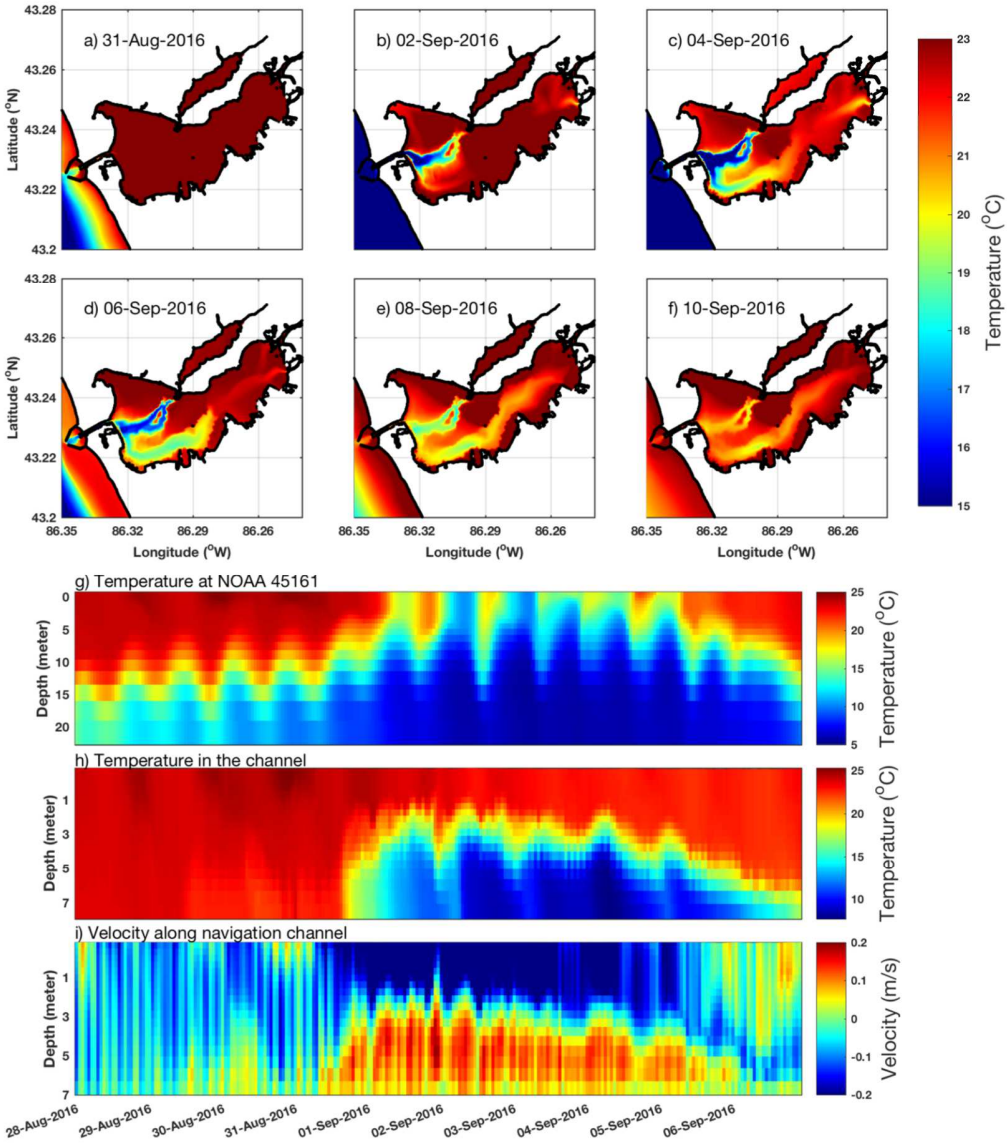

Figure 4. SCHISM model results for the cold-water intrusion event at the beginning of September 2016. a-f) Daily-averaged bottom-temperature during the cold water intrusion event; Hovmöller diagrams for f) temperature at NOAA 45161, g) temperature at the station CHAN in the navigation channel and h) velocity along the navigation channel for the station CHAN in the channel. The positive velocities represent currents moving into MLE, and negative ones represent currents out of MLE.

From September 1 to September 7, the Ekman transport moves surface water away from the eastern shore of Lake Michigan, and replaces the surface water with bottom offshore water, decreasing temperature through the water column near shore, for example, at NOAA 45161 from 25^{o}C to 5^{o}C (Fig. 4g). During upwelling, the Poincaré wave still dominates the thermocline oscillations in Lake Michigan but with lower temperature. The replaced water moving further into the MLE through the connection channel, stratifies the channel's water column with a cold subsurface layer from Lake Michigan waters, and induces a bi-directional flow in the channel, where cold-waters intrude along the bottom half of the channel. As a result of the cold-water intrusion, the surface current strengthens from MLE to Lake Michigan, although the change in net flow was negligible.

The cold-water intrusion first moves northeastward to the northern deep trough toward the mouth of Bear Creek, and then moves gradually southeastward along the southern trough reaching ~80% of MLE (Fig. 4). Around September 6, when downwelling-favorable winds predominate over upwelling-favorable winds, the upwelling along Lake Michigan's coast retreats, leaving the cold-water in MLE and gradually dissipating by mixing. By calculation, the total volume of the cold-water intruded to MLE during the event from September 1 to September 6 is 1.57×10^{7} m^{3}, which is 13% of the Muskegon Lake volume (1.25×10^{8} m^{3} for the SCHSIM model configuration). The net exchange was around 2.2×10^{7} m^{3}, close to the total hydrologic input to MLE during this event at an average flow rate of 40 m^{3}/s.

Although intrusion doesn't significantly alter the net outflow, it initiates the water exchange between Lake Michigan and MLE by bringing oligotrophic water into MLE from the bottom and facilitating stronger mesotrophic outflow to Lake Michigan from the surface. With the occurrence of cold-water intrusion, fewer nutrients and seston are retained in MLE.

According to available studies over MLE (Marko et al., 2013; Weinke et al., 2014), the spatial nutrients/seston distribution from the Muskegon River to Lake Michigan plays a significant role in the system's ecological processes. Therefore, the cold-water intrusion is important for the ecological processes.

4.3 Response to hydrologic input shift

As climate projections reveal intensification of extreme precipitation events over the next century (Donat et al., 2016; Wang et al., 2017), experiments R1 to R4 are used to examine how hydrologic inputs affect cold-water intrusions into the estuary. During the upwelling intrusion at the beginning of September, the averaged flow rates from the Muskegon River for the experiments R1, Ctrl, R2, R3 and R4 are 20, 40, 80, 120, and 160 m^3/s, respectively. For all these experiments, we released a conservative, passive dye at the bottom of the water column inside the jetties on September 1 to track the cold-water intrusion into the estuary. An instantaneous snapshot of the horizontal distribution of the dye tracer on September 5 shows that with an increase in river discharge, the intrusion length decreases (Fig. 5). When the average river discharge becomes 160 m^3/s, the cold-water intrusion is completely suppressed.

We quantified the intrusion difference by the change in water volume into MLE across the navigation channel (Fig. 5f). Halving the river discharge increases the transport of bottom water from Lake Michigan to MLE from ~13% of MLE's total volume to ~18%, while increases in river discharge suppress the volume of Lake Michigan waters entering the estuary. For example, doubling the discharge decreases the intrusion volume to ~8%. When the river discharge increases to 4 times of the original value, the intrusion was suppressed with delivery close to 0. The differences between the river input to MLE and the water leaving MLE through

411 the navigation channel was close to the intrusion volume, with a small net balance keeping the
412 total volume in MLE changes slightly.

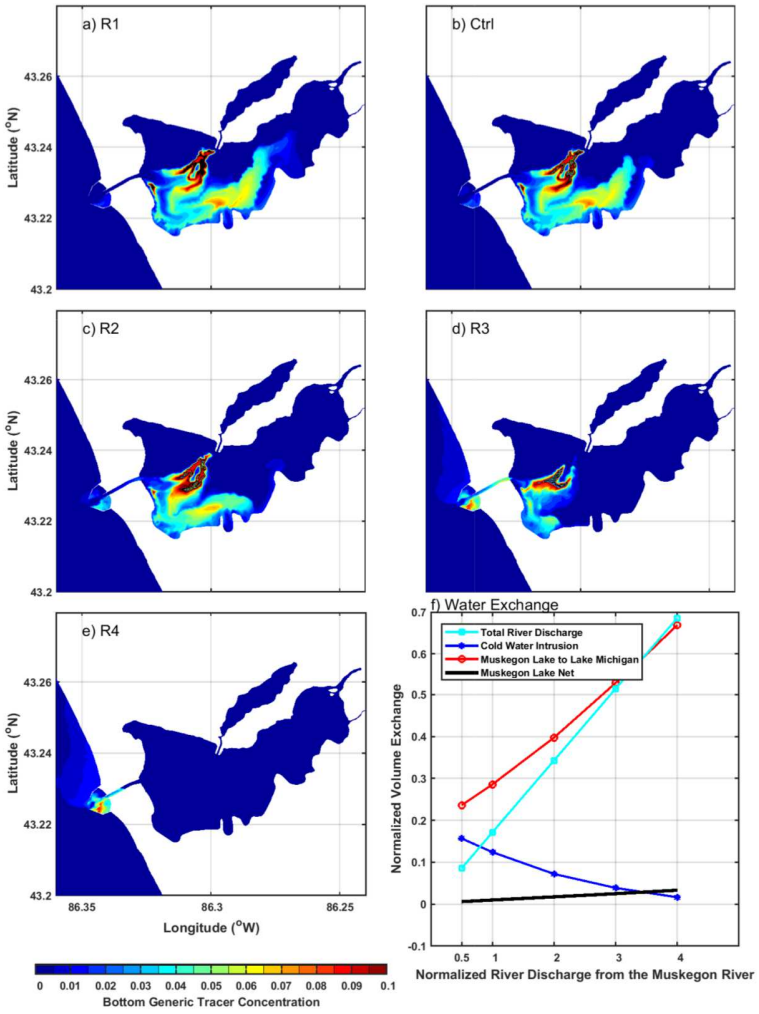

413

414 Figure 5. Model results for the experiments with different hydrologic input during the major
415 upwelling on September 05, 2016 12:00:00, including passive tracer distributions for the
416 experiments a) R1, b) Ctrl, c) R2, d) R3 and e) R4 with normalized river discharges of 0.5, 1, 2,
417 3 and 4, respectively, and f) the corresponding changes in water exchange.

418

419 **4.4 Response to Change in Navigation Channel Width**

420 Experiments N1 and N2 are used to demonstrate the influence of connecting channel
421 characteristics on exchange between drowned river-mouth estuaries and offshore waters. Fig. 6
422 shows the bottom temperature distribution for this set of experiments. With the increase of

navigation channel width, the intrusion length increases. For the case Ctrl (Fig. 6a), waters colder than 15°C stays in the northern trough only, while in the case N2, they reach 1/3 of the total MLE's length.

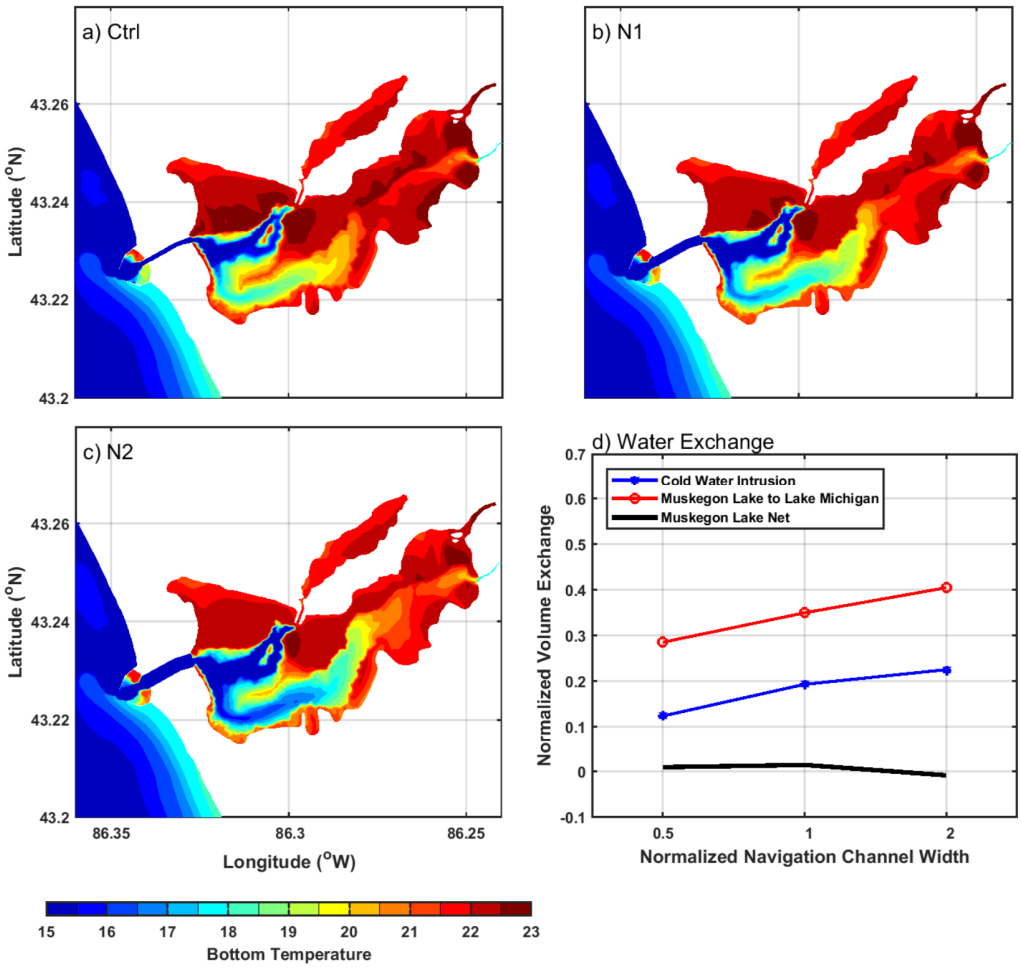

Figure 6. Bottom temperature on September 05, 2016 12:00:00 for the experiments a) Ctrl, b) N1 and c) N2 with normalized navigation channel widths of 1, 2 and 3, respectively, and d) their corresponding changes in water exchange. In N1 and N2, the navigation channel in Ctrl experiment is broadened by 2 and 3 times, respectively.

The intrusion difference was also quantified based on the change in volume flux from Lake Michigan to MLE as shown in Fig. 6d. Compared with the base experiment, doubling the navigation channel width increases the intrusion flux from 13% of Muskegon Lake's volume to

20%, and to 22% if tripling the width. The change of outflow from MLE is proportional to the change in cold-water intrusion, resulting in a small change in the net balance. Despite that, broadening the channel significantly increases the water exchange between Lake Michigan and MLE. This study will provide a good reference for the future studies of other similar brackish or freshwater estuaries that are connected to larger open water bodies with a channel.

4.5. Response to wind conditions

Wind experiments W1 to W3 have wind speeds that are common in Lake Michigan, while W4 has an extreme wind speed as shown in Fig. S5. The Hovmöller diagrams in Figs. 7a-h show the velocity and temperature in the navigation channel. We can see the increase of wind amplitude from 3 m/s in W1 to 7 m/s in W3 strengthens the intrusion with stronger vertical shear in currents and larger temperature stratification. The intrusion flux (Fig. 7i) increased from about 10 m^3/s in W1 to 20 m^3/s in W3, while the net flux to MLE keeps nearly constant. Meanwhile, the onset time of intrusion becomes earlier from W1 to W3 with the increase of wind speed, which resulted from the quick build-up of pressure gradient between offshore and onshore regions. Fig. 7j shows the pressure gradient between two stations on the near shore region of Lake Michigan (ends of the magenta line in Fig. 1b). For W1-3, it increases gradually during the first three days with winds, and then decreases smoothly after winds' disappearance. The intrusion can continue for another several days, dependent on the time needed for pressure restoration. Stronger upwelling generated a longer tail for the intrusion flux; meanwhile the cold-water moved into MLE with a larger intrusion length, i.e., the length that cold-water propagates in MLE (Fig. 8). In W1, the cold-water intrusion was weak and difficult to identify, though in W2 and W3, the intrusion length increased in response to the increase in wind forcing.

Extreme winds can occur along the eastern coast of Lake Michigan, affecting its estuaries'

458 hydrodynamics and ecosystem. For example, when Hurricane Sandy's remnants reached Lake
459 Michigan in October 2012, wind gusts were as strong as 17 m/s. Using an experiment with an
460 extreme wind events for three days, we investigated how the potential extratropical storms affect
461 MLE's cold-water intrusion.

462 In W4, where the applied wind is akin to a northwesterly, alongshore extratropical storm,
463 upwelling along the eastern shore of Lake Michigan is strong. However, due to the strong
464 turbulent mixing in the navigation channel and MLE, during the applied wind storm, the
465 stratification and vertical shear in the channel (Figs. 7g-h) and MLE (Fig. 8) were suppressed.
466 Therefore, the intrusion flux through the channel was weak, even though the pressure gradient
467 perpendicular to the shore is strong. After the removal of winds, the forcing that balances the
468 strong pressure gradient disappear, which drives a strong transient current toward MLE. With the
469 rapid decrease of pressure gradient and the weakening of turbulent mixing, the cold-water
470 intrusion occurred after the removal of winds during the restoration of pressure gradient.

471 Another form of upwelling-favorable wind, offshore wind blowing from the MLE to
472 Lake Michigan, also causes upwelling along the eastern shore of Lake Michigan and cold-water
473 intrusion into the MLE. Because the change of wind speed in offshore wind causes the similar
474 response in cold-water intrusion by the change in alongshore wind, we put the related model
475 results (Fig. S6) and discussion in the Supplementary Material.

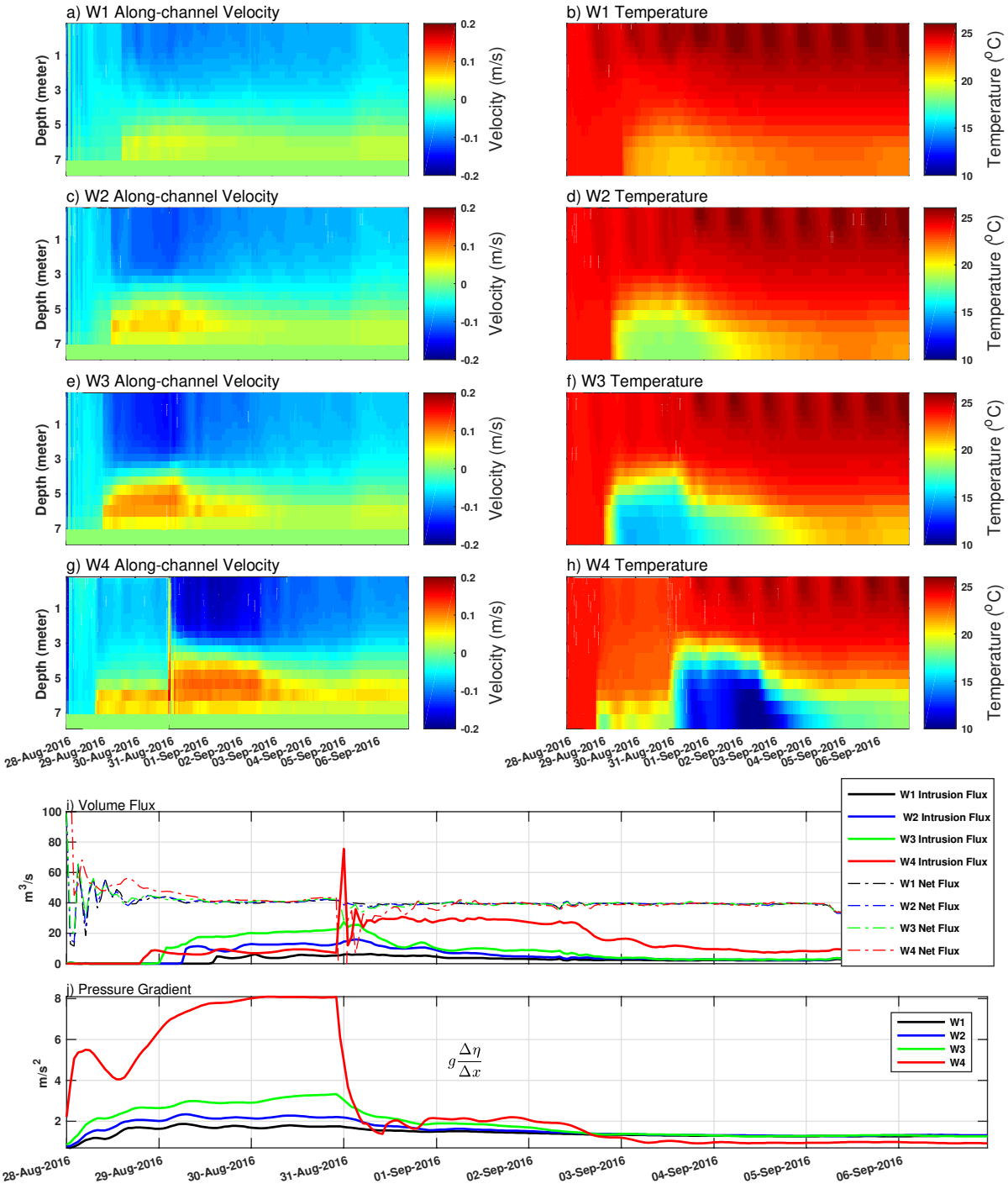

Figure 7. Water exchange between Lake Michigan and MLE from the experiments with prevailing upwelling-favorable winds in different magnitudes of 3, 5, 7 and 15 m/s in W1 to W4. a-h) Hovmöller diagrams for along-channel currents and temperature at the CHAN station for experiments W1 to W4; i) Intrusion flux into MLE (solid lines) and net flux into MLE (dashed lines) for the experiments W1 to W4; j) Pressure gradients between the onshore and offshore points in Lake Michigan close to MLE. The onshore and offshore points in Lake Michigan are the ends of the magenta line shown in Figure 1b.

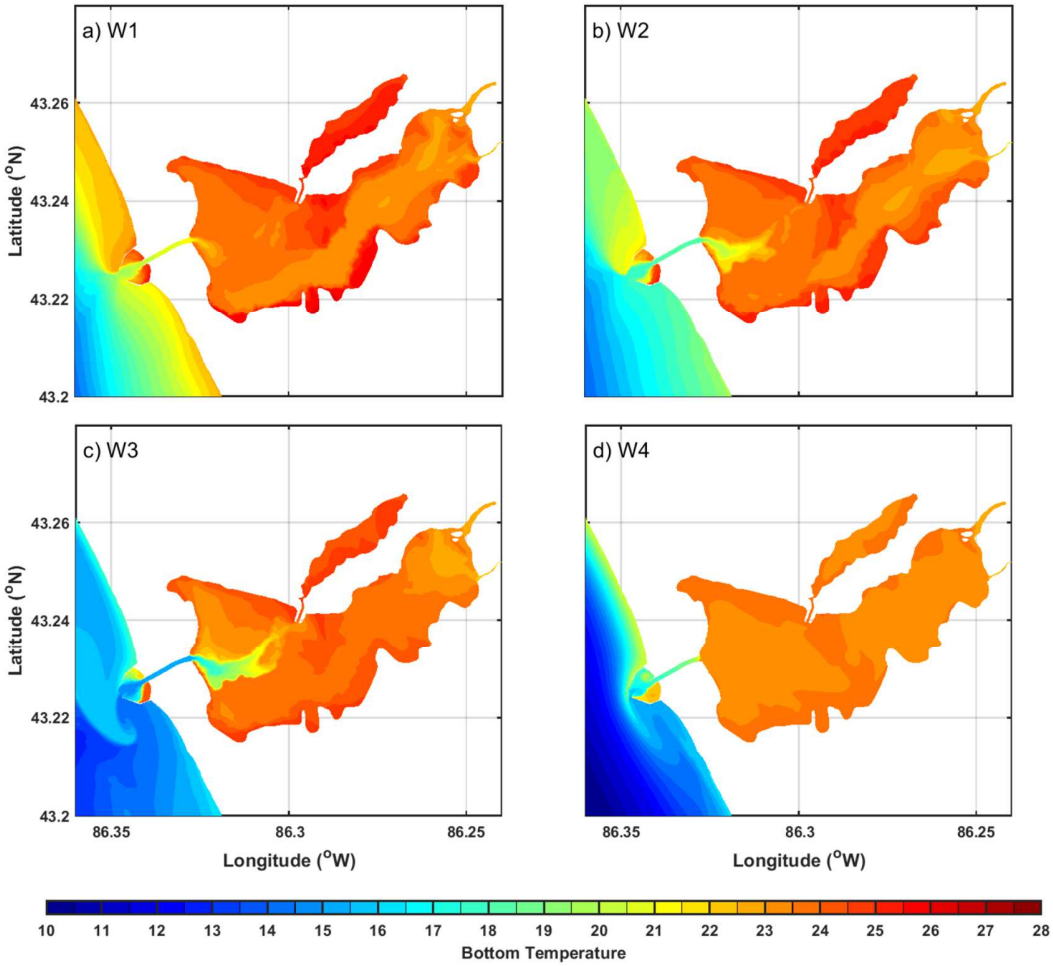

Figure 8. Bottom temperature snapshots on August 30, 2016 12:00:00 for experiments with prevailing upwelling-favorable winds from August 28 to August 30 in a) 3 m/s (W1), b) 5m/s (W2), c) 7 m/s (W3) and d) 15 m/s (W4).

4.6 Frequency of Cold-water Intrusions

Continuous hydrodynamic monitoring in the navigation channel between MLE and Lake Michigan was not established until 2016. Therefore, direct measurements of cold-water intrusion were not available before 2016. However, as a direct consequence of upwelling along the eastern shore of Lake Michigan, the cold-water intrusion can be inferred by the observation of upwelling

at coastal locations. When stratification is established in Lake Michigan, upwelling decreases temperature through the water column; in contrast, downwelling piles up warm surface waters toward the coast, increasing deep water temperature. Buoys deployed in the nearshore Lake Michigan have been recording the near-surface and near-bottom temperature since 2009 (NOAA's National Data Buoy Center Station 45161; http://www.ndbc.noaa.gov/). Therefore, we could analyze the temperature anomalies to identify upwelling along the eastern shore of Lake Michigan and, hence, the cold-water intrusion to MLE.

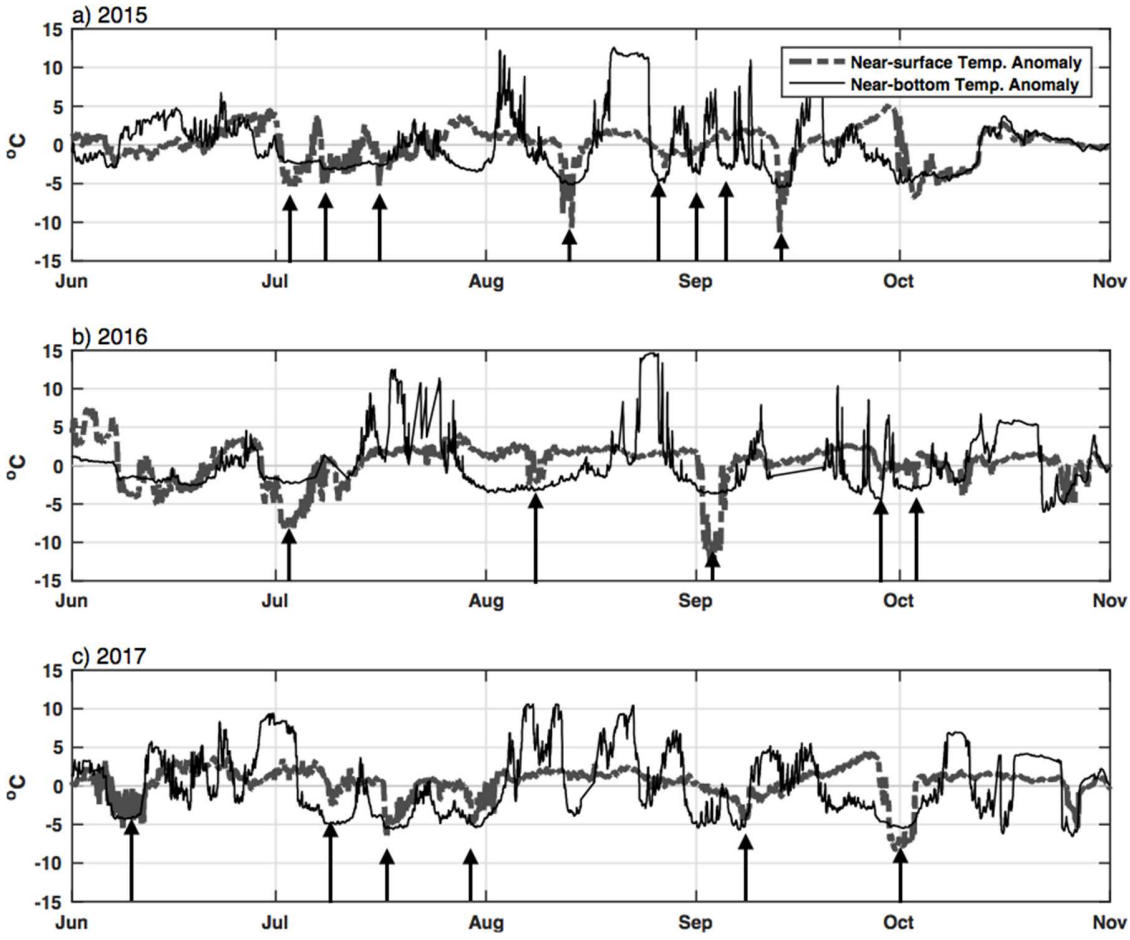

Figure 9. Anomalies of surface temperature and bottom temperature measured at the NOAA 45161 station in a) 2015, b) 2016 and c) 2017. A high-pass filter with a cut-off period of 1 month was used to remove the seasonal trend. Arrows indicate periods of potential upwelling.

509 Fig. 9 shows the near-surface (dashed lines) and near-bottom (solid lines) temperature
510 anomalies, the temperature variation by removing seasonal trend, at station 45161 from 2015 to
511 2017. An upwelling event is established accompanied by the decrease of both near-bottom and
512 near-surface temperature. When the upwelling doesn't have enough duration or strength, the
513 near-surface temperature anomaly is small. We marked the potential upwelling-caused water
514 anomalies as upward arrows in Fig. 8. The intrusions were likely to occur at least once from June
515 to November in 2015 and 2016, and likely more prevalent in 2017. The temperature anomalies in
516 July 2017 show 3 upwelling events spanning the whole month. The duration of cold-water
517 intrusion is mostly determined by the upwelling duration according to the previous analysis. Fig.
518 9 shows that the cold-water intrusion can last as long as weeks. For example, the intrusion in
519 August 2016 lasted about 3 weeks, and the intrusion at the beginning of September 2016 lasted
520 for a week. However, there is risk to counting the intrusion duration solely by the upwelling
521 duration, because the intrusion is susceptible to the river flow suppression and strong wind
522 mixing in the channel.

523 **4.7 Model Limitations**

524 Groundwater is another important natural input to the Great Lakes, accounting for 1-12%
525 of total water inflow to Lake Michigan (Robinson, 2015), as well as to the freshwater estuary of
526 MLE along Lake Michigan. However, due to the statistical variability and methodological
527 inaccuracies associated with the monitoring efforts, groundwater data is scarce and imprecise
528 (Mitchell et al., 1988). To examine the impact of groundwater flux to the hydrodynamics of
529 MLE, we arbitrarily added 20 groundwater sources along the deepest locations in the eastern
530 reach of the MLE (marked in Fig. S7) with a total constant flux of 20 m^3/s and temperature of
531 8^oC. According to Collins (1925), the approximate average temperature of shallow groundwater

obtained from shallow wells in western Michigan ranges from 8°C to 11°C. In the idealized experiment, we used even lower temperature for the highly sparse groundwater sources. The modeled temperature (Fig. S8) shows significant improvement in bottom temperature and stratification. The idealized experiment demonstrates the groundwater flux could significantly increase MLE's stratification. Although the groundwater input may play an important role in the MLE's ecosystem, as a potential source of nutrients that stimulates algal blooms (Kilroy and Coxon, 2005; Lewandowski et al., 2015; Knights et al., 2017), its effect on timing and duration of cold-water intrusion is small (Fig. S9). However, it can slightly decrease the volume of the intrusion (around 10%) according to the time series of cold-water intrusion flux (Fig. S10). Further improvement of the SCHISM model with realistic groundwater sources will be conducted in the future.

5. Summary and Conclusions

We used a 3-D hydrodynamic model (SCHISM) to study the water exchange between Lake Michigan and a freshwater estuary. The model successfully captures the episodic cold-water intrusions driving by upwelling events in Lake Michigan. As a result of Ekman transport, the upwellings deliver a large volume of cold-water to MLE, resulting in a significant impact on the hydrodynamics of the freshwater estuary. For example, the upwelling at the beginning of September 2016 induced a cold-water intrusion with a volume near 13% of the entire MLE. For the first time, near-surface and near-bottom temperature anomalies at NDBC 45161, a NOAA buoy along Lake Michigan's eastern shore, are analyzed to indirectly identify the occurrence of cold-water intrusion from Lake Michigan to MLE. The results reveal that the cold-water intrusion to MLE is common, which appears a least once per month with duration from days to

555 weeks, determined by the duration and strength of the upwelling-favorable winds.

556 In addition to hydrodynamic implications, these intrusions exchange biologically distinct
557 waters between Lake Michigan and MLE. Compared with MLE, waters in Lake Michigan
558 contain less organic matter, total suspended matter, and total phosphorus of fine sediment, but
559 more dissolved oxygen. To conserve the volume in MLE, the cold-water intrusion from Lake
560 Michigan to MLE along the lake bottom is accompanied by a stronger surface outflow.
561 Therefore, the intrusion not only dilutes the related matter and nutrients in MLE but also
562 accelerates their transport out of MLE. Furthermore, Biddanda et al. (2018) suggested that the
563 episodic cold-water intrusion affects the MLE's ecosystem by bringing water with more
564 dissolved oxygen to the estuary bottom, mitigating summer hypoxia for a short period of time, in
565 contrast to the commonly-observed intrusion of hypoxic waters from coastal oceans into brackish
566 estuaries (Deppe, 2017; Rabalais, 2002; Breitburg, 1992; Breitburg, 2002; Sanford et al., 1990;
567 Levin et al., 2009).

568 Through process-oriented experiments, we examined the cold-water intrusion's responses
569 to hydrological shift, variation in navigation channel width, and wind conditions. It is found that
570 the increase in riverine input during the upwelling weakens the intrusion. Marko et al. (2013)
571 suggested the increase in river discharge brings more organic matter, total suspended matter,
572 total phosphorus and sediment into MLE, while our study demonstrates the suppression of the
573 intrusion by the increase in river discharge. The suppression may deteriorate the water quality by
574 retaining more organic matter and nutrients in MLE – including summer time surface blooms of
575 harmful cyanobacteria. This would suggest that a hydrologic shift under a changing climate
576 would alter the ecosystem through affecting the water exchange between Lake Michigan and
577 MLE. The conclusion may provide a good reference to the study of estuaries whose physical and

578 ecological processes are susceptible to upwelling-downwelling wind cycle and changing
579 hydrological conditions, for example, San Francisco Bay (Liu et al., 2018), Chesapeake Bay
580 (Breitburg, 1992; 2002), the Columbia River Estuary (Roegner, 2001), Willapa Bay (Roegner,
581 2002), etc.

582 In addition, the present work shows that the extent and strength of intrusion depends on
583 the structure of the connecting pathways between the estuary and the offshore waters. Results
584 show that the increase of navigation channel width strengthens the cold-water intrusion, which is
585 not only important for extrapolation of these results to other freshwater estuaries, but may also be
586 important for management and coastal engineering projects in similar systems with narrow
587 channels (for example, Tampa Bay, Zhu et al., 2014).

588 Through experiments with different wind speeds in the along-shelf direction, we further
589 investigated the dynamics behind the intrusion. Stronger upwelling causes a stronger and longer
590 duration intrusion with larger intrusion length into MLE. Driven by the pressure gradient
591 between onshore and offshore, the cold-water intrusion doesn't disappear right after the absence
592 of upwelling-favorable winds, but instead dissipates gradually with the relaxation of the pressure
593 gradient. When extreme upwelling-favorable winds occur (for example, during extratropical
594 storms, winds can reach 15 m/s), the intrusion during the winds is weak. However, the strong
595 upwelling caused by the extreme winds continues to work after the winds absence with an even
596 stronger intrusion to MLE.

597 Overall, cold-water intrusions may be critical for optimal water exchange and ecosystem
598 function of temperate freshwater estuaries. Such hydrodynamic connectivity may be especially
599 relevant in systems such as the Great Lakes or in the world's coastal estuaries where tidal forcing
600 is weak, including White Lake, Pentwater Lake and Lake Macatawa along the eastern shore of

Lake Michigan, Hamilton Harbour (Lawrence et al., 2004), Frechman's Bay, and White Harbour along Lake Ontario, etc. The frequency and extent of these intrusions depends on a number of factors. However, the present work suggests that under shifting conditions, such as winds and precipitation events or intensity, the critical delivery of nutrients and other water quality components can be altered dramatically, potentially eliminating the replenishment of high dissolved-oxygen and low nutrient intrusions and exacerbating both hypoxic and eutrophic conditions in estuaries.

Acknowledgements:

We thank the NOAA-Great Lakes Environmental Research Laboratory (GLERL)'s Lake Michigan Field Station for providing logistical ship-support with yearly Muskegon Lake Observatory buoy (MLO) deployment and recovery operations. The MLO infrastruture and open access data that were utilized in this study was funded by EPA Great Lakes Restoration Initiative, NASA Michigan Space Grants Consortium and University of Michigan-Cooperative Institute for Great Lakes Research (CIGLR) grants to BB. We are grateful to Steve Ruberg, NOAA-GLERL for open access data from NOAA's nearshore Lake Michigan buoy (NOAA 45161). A Community Foundation for Muskegon County grant to the Annis Water Resources Institute supported the long-term seasonal ship-board monitoring of Muskegon Lake. We thank Kurt Thompson and Alan Steinman, Annis Water Resources Institute, Grand Valley State University for providing regional groundwater data for analysis. QL acknowledges the support from a CIGLR postdoctoral fellowship award to BB and EA. This is CIGLR publication #_____ and GLERL publication #_____.

References:

Anderson E. J. and Schwab, D. J. (2011) Relationships between wind-driven and hydraulic flow in Lake St. Clair and the St. Clair River Delta. *J. Great Lakes Res.*, 37, 147-158.

Anderson E. J. and Schwab, D. J. (2017) Meteorological influence on summertime baroclinic exchange in the Straits of Mackinac. *J. Geophys. Res. Oceans* **122**:3, 2171-2182.

Allan JD, McIntyre PB, Smith SDP, Halpern BS, Boyer GL, Buchsbaum A, Burton Jr. GA, Campbell LM, Chadderton WL, Ciborowski JJH, Doran PJ, Eder T, Infante DM, Johnson LB, Joseph CA, Marino AL, Prusevich A, Read JG, Rose JB, Rutherford ES, Sowa SP, Steinman AD. (2012). Joint analysis of stressors and ecosystem services to enhance restoration effectiveness. *Proc Natl Acad Sci U. S. A.*, 110: 372-377.

Borja, Á., Dauer, D.M., Elliott, Simenstad, C.A. (2010). Medium- and long-term recovery of estuarine and coastal ecosystems: patterns, rates and restoration effectiveness. *Estuar. Coasts*, 33, 1249–1260.

Biddanda, B. A. (2012). Lake Sentinel: Observatory for Ecosystem Changes in Muskegon Lake. *InterChange*, Newsletter of Regional Math and Science Center, Grand Valley State University. http://www.gvsu.edu/rmsc/interchange/2012-may-connections-awri-651.htm

Biddanda, B. A, A. D. Weinke, S. T. Kendall, L. C. Gereaux, T. M. Holcomb, M. J. Snider, D. K. Dila, S. A. Long, C. VandenBerg, K. Knapp[1], D. J. Koopmans, K. Thompson, J. H. Vail, M. E. Ogdahl, Q. Liu, T. J. Johengen, E. J. Anderson, and S. A. Ruberg (2018). Chronicles of Hypoxia: Time-series buoy observations reveal annually recurring seasonal basin-wide hypoxia in Muskegon Lake – a Great Lakes estuary, *J. Great Lakes Res.*, 44(2), 219-229. https://doi.org/10.1016/j.jglr.2017.12.008.

646 Biddanda, B.A. (2017) Global significance of the changing freshwater carbon cycle. Eos,
647 American Geophysical Union 98(6): 15-17. https://doi.org/10.1029/2017EO069751
648 Beletsky, D., W. P. O'Connor, D. J. Schwab, and D. E. Dietrich. (1997) Numerical simulation of
649 internal kelvin waves and coastal upwelling fronts, *J. Phys. Oceanogr.*, **27**, 1197–1215.
650 Beletsky, D., J. H. Saylor, and D. J. Schwab. (1999) Mean circulation in the Great Lakes, *J.*
651 *Great Lakes Res.*, **25**(1), 78–93.
652 Beletsky, D., and D. J. Schwab. (2001) Modeling circulation and thermal structure in Lake
653 Michigan: Annual cycle and interannual variability, *J. Geophys. Res.*, 106, 19745-19771.
654 Breitburg, DL. (1992) Episodic hypoxia in the Chesapeake Bay: interacting effects of
655 recruitment, behavior and a physical disturbance, *Ecol. Monograph.*, 62, 525–546, 1992.
656 Breitburg DL. (2002) Effects of hypoxia, and the balance between hypoxia and enrichment, on
657 coastal fishes and fisheries. *Estuaries*, 25, 767. https://doi.org/10.1007/BF02804904
658 Chao, Y., Farrara, J. D., Zhang, H., Zhang, Y. J., Ateljevich, E., Chai, F., Davis, C.O., Dugdale,
659 R., & Wilkerson, F. (2017) Development, implementation, and validation of a modeling
660 system for the San Francisco Bay and estuary. *Estuar., Coast. Shelf Sci.*,
661 https://doi.org/10.1016/j.ecss.2017.06.005.
662 Chen S-N, WR Geyer, DK Ralston, and JA Lerczak. (2012) Estuarine exchange flow quantified
663 with isohaline coordinates: contrasting long and short estuaries, *J. Phys. Oceanogr.*, 42,
664 748-763, doi: 10.1175/JPO-D-11-086.1.
665 Collins, W.D. (1925) Temperature of Water Available for Industrial Use in the United States
666 1923–1924. In: Contributions to the hydrology of the United States, Water supply paper
667 520, Chapter F.. United States Geological Survey, Washington, DC, pp. 97–104.
668 Cotner, J.B., A.D. Weinke, and B.A. Biddanda. 2017. Great Lakes: Science can keep them

669 great. *J. Great Lakes Res.*, 43: 916-919. https://doi.org/10.1016/j.jglr.2017.07.002
670 Deppe, R.W., Thomson, J., Polagye, B. et al. (2017) Predicting Deep Water Intrusions to Puget
671 Sound, WA (USA), and the Seasonal Modulation of Dissolved Oxygen. *Estuaries and*
672 *Coasts*, 1-14. https://doi.org/10.1007/s12237-017-0274-6.
673 Donat, M. G., Lowry, A. L., Alexander, L. V., O'Gorman, P. A., & Maher, N.. (2016) More
674 extreme precipitation in the world's dry and wet regions, Nature Climate Change, 6, 508–
675 513. doi:10.1038/nclimate2941.
676 Ekman, V.W. (1905) On the influence of the earth's rotation on ocean currents. *Ark. Mat. Astron.*
677 *Fys.*, 2 (11): 1–52.
678 Fisher J.C, Newton R.J, Dila D.K, and McLellan S.L. (2015) Urban microbial ecology of a
679 freshwater estuary of Lake Michigan. *Elem. Sci. Anth.*, 2015;3:64.
680 DOI:http://doi.org/10.12952/journal.elementa.000064.
681 Geyer, WR, DK Ralston. (2015) Estuarine frontogenesis. *J. Phys. Oceanogr.*, 45(2): 546-
682 561, doi:10.1175/JPO-D-14-0082.1.
683 Grunert, Brice. (2013) Evaluating the Summer Thermal Structure of Southern Green Bay, Lake
684 Michigan. Theses and Dissertations. 252. https://dc.uwm.edu/etd/252.
685 Hecky R. E. , Campbell P. , Hendzel L. L. (1993) The stoichiometry of carbon, nitrogen, and
686 phosphorus in particulate matter of lakes and oceans, *Limnol. and Oceanogr.*, 38, doi:
687 10.4319/lo.1993.38.4.0709.
688 Hoffman, B. M., Lukoyanov, D., Yang, Z.-Y., Dean, D. R., & Seefeldt, L. C. (2014) Mechanism
689 of Nitrogen Fixation by Nitrogenase: The Next Stage. *Chemical Reviews*, *114*(8), 4041–
690 4062. http://doi.org/10.1021/cr400641x.

691 Kantha, L.H. and C.A. Clayson. (1994) An improved mixed layer model for geophysical
692 applications. *J. Geophy. Res.*, 99(25), pp. 235-266.
693 Knights, D., K. C. Parks, A. H. Sawyer, C. H. David, T. N. Browning, K. M. Danner, and C. D.
694 Wallace, (2017) Direct groundwater discharge and vulnerability to hidden nutrient loads
695 along the Great Lakes coast of the United States. *J. Hydrol.*, 554, pp. 331-341.
696 Kilroy, G., and Coxon, C., (2005) Temporal variability of phosphorus fractions in Irish karst
697 springs. *Environ. Geol.*, 47, 421-430.
698 Larson, J.H., Trebitz, A.S., Steinman, A.D., Wiley, M.J., Mazur, M.C., Pebbles, V., Braun, H.A.,
699 Seelbach, P.W. (2013) Great Lakes rivermouth ecosystems: scientific synthesis and
700 management implications. *J. Great Lakes Res.*, 39, 513–524.
701 Lawrence, G., Pieters, R., Zaremba L., Tedford, T., Gu, L., Greco, S., and Hamblin, P. (2004)
702 Summer exchange between Hamilton Harbour and Lake Ontario. *Deep. Res. Part II Top.*
703 *Stud. Oceanogr.,* 51:475–487.
704 Levin, L. A., Ekau, W., Gooday, A. J., Jorissen, F., Middelburg, J. J., Naqvi, S. W. A., Neira, C.,
705 Rabalais, N. N., and Zhang, J. (2009) Effects of natural and human-induced hypoxia on
706 coastal benthos, *Biogeosciences*, 6, 2063-2098, https://doi.org/10.5194/bg-6-2063-2009,
707 2009.
708 Lewandowski, J., Meinikmann, K., Nutzmann, G., Rosenberry, D. O. (2015) Groundwater – the
709 disregarded component in lake water and nutrient budgets. Part 2: effects of groundwater
710 on nutrients. *Hydrol. Process.*, 29, 2922-2955.
711 Liu, Q., Rothstein, L. M., Luo, Y., Ullam, D.S., & Codiga, D. L. (2016a) Dynamics of the
712 periphery current in Rhode Island Sound. *Ocean Model.*, 105, 13-24.
713 https://doi.org/10.1016/j.ocemod.2016.07.001.

714 Liu, Q., Rothstein, L. M., & Luo, Y. (2016b) Dynamics of the Block Island Sound estuarine
715 plume. *J. Phys. Oceanogr.*, 46 (5), 1633–1656. https://doi.org/10.1175/JPO-D-15-0099.1.
716 Liu, Q., L. M. Rothstein, and Y. Luo. (2017) A periodic freshwater patch detachment process
717 from the Block Island Sound estuarine plume, *J. Geophys. Res. Oceans*, 122, 570–586,
718 doi:10.1002/2015JC011546.
719 Liu, Q., F. Chai, R. Dugdale, Y. Chao, H. Xue, S. Rao, F. Wilkerson, J. Farrara, H. Zhang, Z.
720 Wang, and Y. J. Zhang. (2018) San Francisco Bay Nutrients and Plankton Dynamics as
721 Simulated by a Coupled Hydrodynamic-Ecosystem Model. *Cont. Shelf Res.*,
722 https://doi.org/10.1016/j.csr.2018.03.008.
723 Marko, K. M., Rutherford, E. S., Eadie, B. J., Johengen, T.H., and Lansing, M.B. (2013)
724 Delivery of nutrients and seston from the Muskegon River Watershed to near shore Lake
725 Michigan. *J. Great Lakes Res.*, 39:672–681.
726 Mitchell, D.F., Wagner, K.J., and Asbury, C. (1988) Direct measurement of groundwater flow
727 and quality as a lake management tool. *Lake and Reservoir Management*, 4: 169–178.
728 Mortimer, C.H. (1984) Measures and models in physical limnology. In: Hydrodynamics of Lakes
729 (K. Hutter Ed) CISM Courses and Lectures Nr 286, Springer Verlag Vienna-New York:
730 287-322.
731 Mortimer, C. H. (2004) Lake Michigan in Motion. Earth-Spin, and Human Activities, The
732 University of Wisconsin Press: 173-196.
733 Pitcher, G. C., Figueiras, F. G., Hickey, B. M., & Moita, M. T. (2010) The physical
734 oceanography of upwelling systems and the development of harmful algal blooms. *Prog.*
735 *Oceanogr.*, 85(1-2), 5–32. http://doi.org/10.1016/j.pocean.2010.02.002.

Plattner, S., Mason, D. M., Leshkevich, G. A., Schwab, D. J., Rutherford, E. S. (2006) Classifying and forecasting coastal upwellings in Lake Michigan using satellite derived temperature images and buoy data. *J. Great Lakes Res.*, 32(1), 63-76, ISSN 0380-1330, https://doi.org/10.3394/0380-1330(2006)32[63:CAFCUI]2.0.CO;2.

Rabalais, Nancy N., R. Eugene Turner, William J. Wiseman Jr. (2002) Gulf of Mexico Hypoxia, A.K.A. "The Dead Zone". *Annu. Rev. Ecol. Syst.*, 33:1, 235-263.

Roegner, G.C., J.A. Needoba, & A.M., Baptista. (2011) Coastal upwelling supplies oxygen-depleted water to the Columbia River estuary. *PLoS ONE*, 6(4): e18672. https://doi.org/10.1371/journal.pone.0018672.

Roegner, G.C., B.M. Hickey, J.A. Newton, A.L. Shanks, and D.A. Armstrong. (2002) Wind-induced plume and bloom intrusion into Willapa Bay, Washington, *Limnol, Oceanogr.*, 47(4), 1033-1042. https://doi.org/10.4319/lo.2002.47.4.1033.

Rong, Z., and M. Li. (2012) Tidal effects on the bulge region of Changjiang River plume, *Estuar., Coast. Shelf Sci.*, 97, 149–160, doi:10.1016/j.ecss.2011.11.035.

Safaie, A., Litchman, E., & Phanikumar, M. S. (2017) Evaluating the role of groundwater in circulation and thermal structure within a deep inland lake. *Adv. in Water Resour.*, *108*, 310-327. DOI: 10.1016/j.advwatres.2017.08.002.

Sanford, L.P, Sellner K.G, Breitburg D.L. (1990) Covariability of dissolved oxygen with physical processes in the summertime Chesapeake Bay. *J. Mar. Res.*, 48:567-90.

Schwab, D. J. (1983) Numerical simulation of low-frequency current fluctuations in Lake Michigan. *J. Phys. Oceanogr.* 13, 2213-2224.

Schwab, D. J., and J. R. Bennett. (1987) Lagrangian comparison of objectively analyzed and dynamically modeled circulation patterns in Lake Erie. *J. Great Lakes Res.* 13, 515-541.

759 Schwab, D. J., and K. W. Bedford. (1994) Initial implementation of the Great Lakes Forecasting
760 System: A real-time system for predicting lake circulation and thermal structure, *Water*
761 *Pollut. Res. J. Can.*, **29**(2/3), 203–220.
762 Schwab, D. J. (1977) Internal free oscillations in Lake Ontario. Limnol. Oceanogr., 22, 700-708.
763 Simpson, J. H., J. Brown, J. Matthews and G. Allen. (1990) Tidal straining, density currents, and
764 stirring in the control of estuarine stratification, *Estuaries*, 13(2), 125–132.
765 Sinha, E., A. M. Michalak and V. Balaji. (2017) Eutrophication will increase during the 21st
766 century as a result of precipitation changes. *Science*, 357, 405-408.
767 Steinman A. D., Ogdahl M., Rediske R., Ruetz III C.R., Biddanda, B. A., and Nemeth L. (2008)
768 Current status and trends in Muskegon Lake, Michigan. *J. Great Lakes Res.*, 34:169–188.
769 Tang, Z., B.A. Engel, B.C. Pijanowski, and K.J. Lim. (2005) Forecasting land use change and its
770 environmental impact at a watershed scale. *J. Environ. Manage.*, 76(2): 35-45.
771 Tranvik Lars J. , Downing John A. , Cotner James B. , Loiselle Steven A. , Striegl Robert
772 G. , Ballatore Thomas J. ,Dillon Peter , Finlay Kerri , Fortino Kenneth , Knoll Lesley
773 B. , Kortelainen Pirkko L. , Kutser Tiit , Larsen Soren. , Laurion Isabelle , Leech Dina
774 M. , McCallister S. Leigh , McKnight Diane M. , Melack John M. , Overholt Erin ,Porter
775 Jason A. , Prairie Yves , Renwick William H. , Roland Fabio , Sherman Bradford
776 S. , Schindler David W. ,Sobek Sebastian , Tremblay Alain , Vanni Michael
777 J. , Verschoor Antonie M. , von Wachenfeldt Eddie ,Weyhenmeyer Gesa A. (2009) Lakes
778 and reservoirs as regulators of carbon cycling and climate. *Limnol. Oceanogr.*, 54, doi:
779 10.4319/lo.2009.54.6_part_2.2298.
780 Umlauf, L. and H. Burchard. (2003) A generic length-scale equation for geophysical turbulence
781 models. *J. Mar. Res.*, 6, pp. 235-265.

782 Wang, G., D. Wang, K.E. Trenberth, A. Erfanian, M. Yu, M. G. Bosilovich and D. T. Parr. (2017)
783 The peak structure and future changes of the relationships between extreme precipitation
784 and temperature, *Nature Climate Change*, 7, 268-274. Doi:10.1038/nclimate3239.
785 Weinke A.D, Kendall, S.T, Kroll, D.J, Strickler, E.A, Weinert, M.E, Holcomb, T.M, Defore,
786 A.A, Dila, D.K, Snider ,M.J, Gereaux, L.C, Biddanda, B.A., (2014) Systematically
787 variable planktonic carbon metabolism along a land-to-lake gradient in a Great Lakes
788 coastal zone. J. Plankton. *Res.*, 36: 1528–1542.
789 Weinke A.D. and B.A. Biddanda. (2018) From bacteria to fish: Ecological consequences of
790 seasonal hypoxia in a Great Lakes estuary. *Ecosystems*, 21(3), 426-442.,
791 https://doi.org/10.1007/s10021-017-0160-x.
792 Wiley, M.J., Hyndman, D.W., Pijanowski, B.C. et al. (2010). A multi-modeling approach to
793 evaluating climate and land use change impacts in a Great Lakes River Basin.
794 *Hydrobiologia*, 657: 243. https://doi.org/10.1007/s10750-010-0239-2.
795 Zhang, Y., and Baptista, A.M. (2008) SELFE: A semi-implicit Eulerian-Lagrangian finite-
796 element model for cross-scale ocean circulation. *Ocean Model.*, 21(3-4), 71-96.
797 Zhang, Y. J., Witter, R. C., & Priest, G. R. (2011) Tsunami–tide interaction in 1964 Prince
798 William Sound tsunami. *Ocean Model.*, *40*(3–4), 246–259.
799 https://doi.org/10.1016/j.ocemod.2011.09.005.
800 Zhang, Y., Ateljevich, E., Yu, H-C., Wu, C-H., & Yu, J.C.S. (2015) A new vertical coordinate
801 system for a three-dimensional unstructured-grid model, *Ocean Model.*, **85**, 16-31.
802 Zhang, Y., Ye, F., Stanev, E.V., & Grashorn, S. (2016) Seamless cross-scale modeling with
803 SCHISM, *Ocean Model.*, 102, 64-81. doi:10.1016/j.ocemod.2016.05.002.
804